Aberystwyth University

The Earth Observation-based Anomaly Detection (EOAD) system
Castillo-villamor, Liliana; Hardy, Andy; Bunting, Pete; Llanos-peralta, Willian; Zamora, Miguel; Rodriguez, Yeison; Gomez-latorre, Douglas A.

The Earth Observation-based Anomaly Detection (EOAD) system: A simple, scalable approach to mapping in-field and farm-scale anomalies using widely available satellite imagery

Liliana Castillo-Villamor [a,*], Andy Hardy [a], Pete Bunting [a], Willian Llanos-Peralta [c], Miguel Zamora [b], Yeison Rodriguez [b], Douglas A. Gomez-Latorre [d]

[a] *Earth Observation and Ecosystems Dynamics Research Group, Department of Geography and Earth Sciences, Aberystwyth University, United Kingdom*
[b] *Hacienda El Escobal, Ibague, Colombia*
[c] *Universidad Nacional de Colombia, Bogotá, Colombia*
[d] *Corporacion colombiana de investigacion agropecuaria (AGROSAVIA), Colombia*

A R T I C L E I N F O

A B S T R A C T

To feed the world increasing population, expansion in the area under arable cultivation is expected, with the majority projected to occur in Sub-Sahara Africa and Latin American countries. However, many existing Precision Agriculture (PA) techniques are difficult to transfer to agricultural systems in these regions as they rely on prohibitively expensive crop monitoring systems. Satellite Earth Observation (EO) has the ability to provide affordable solutions, particularly to identify yield-limiting conditions within site-specific management zones (MZs). This paper presents the Earth Observation-based Anomaly Detection (EOAD) approach, a novel system for the detection of in-field anomalies through automatic thresholding of optical Vegetation Index data, based on their deviation from a normal distribution. The EOAD sets dynamic thresholds for the pixel values within a parcel by removing the atypical values in increments from the tails towards the median until the distribution is normal. The distribution normality is assessed based upon measures of skewness and kurtosis for each iteration. The anomaly detection approach demonstrated a strong agreement, 80% overall accuracy, with identified in-field anomalies when applied to rice plots in the Ibague Plateau, Colombia, using both Sentinel-2 and PlanetScope imagery. Areas identified as anomalous during the booting stage were shown to be significantly ($p \leqslant 0.005$) associated with a decrease in final yield. Additionally, the percentage of anomalies detected with the EOAD improved the detection of underperforming plots in early growth stages. Using freely available data and software, this automated approach demonstrates an exciting potential for use in improving agricultural practices in low-resource regions.

1. Introduction

Projections indicate that by 2050 arable land is estimated to increase by 12% in low-income countries compared to 2009 levels (Alexandratos and Bruinsma, 2012; Kirova et al., 2019). Adopting environmentally sustainable cropping systems in these regions is crucial to increase resistance to environmental stress, enhanced crops nutritional content, and, ultimately, safeguard food supplies in a changing world. However, the adoption of Precision Agriculture (PA) technologies has been slow (Joint Research Centre of the European Commission, 2014). The high-tech nature of traditional PA technologies, developed in advanced countries, involves quantifying biophysical parameters to characterise the very particular conditions of an agricultural system, making it difficult to transfer to others (Delgado et al., 2019; Joint Research Centre of the European Commission, 2014). Nevertheless, rapid changes in the socio-economic conditions of the developing World coupled with demands from specialised markets call for the development of softer PA approaches that are both scalable and transferable (Mondal and Basu, 2009).

A more affordable approach to achieve PA goals is the

---

implementation of agricultural practices based on site-specific management zones (MZs) (Gavioli et al., 2019; Koch et al., 2004; Méndez-Vázquez et al., 2019). These are anomalous areas within a field that have yield-limiting factors (Ye et al., 2007). Gavioli et al. (2019) found that applying a multivariate spatial analysis based on Moran's index and spatially weighted Principal Component Analysis (sPCA) on yield, soil physical properties and topographic data facilitated to define highly homogeneous management zones in corn and soybean crops, in Brazil. However, early detection of anomalous areas is challenging due to their sporadic nature (both in time and space) and lack of clearly visible symptoms without close observation, demanding frequent and detailed ground inspection (Shaw and Kelley, 2005).

The identification of anomalous areas within crop fields using Remote Sensing (RS) has been successfully used to improve agricultural practices (Pérez et al., 2000; Shaw and Kelley, 2005). However, approaches have largely relied on the use of aerial imagery and near-ground sensors at a cost that is prohibitive to many farmers, particularly in resource-poor regions of the World. Satellite Earth Observation (EO) has the potential to support in-field crop anomaly detection reducing frequent detailed scouting, but due to its relatively coarse spatial resolution, satellite EO has mainly been used at regional scales, ignoring in-field variability. For example, medium spatial resolution satellite imagery, such as Landsat (30 m), have been used primarily to map land cover change within agricultural areas rather than monitoring anomalies within crops (e.g. Dutrieux et al., 2016). Also, studies that analyse temporal patterns of crop growth are usually performed with higher frequency imagery, such as Moderate Resolution Imaging Spectroradiometer (MODIS) and SPOT Vegetation (SPOT-VGT) (e.g. Bolton and Friedl, 2013; Eerens et al., 2014; Funk and Budde, 2009; Lasaponara, 2006; Rembold et al., 2019), at a sacrifice of spatial resolution (MODIS:250 m, SPOT-VGT: 1000 m) and are therefore limited to making assessments at regional and global scales (Bolton and Friedl, 2013; Eerens et al., 2014; Lasaponara, 2006), rather than informing sub-plot farm management decisions.

The pixel-based nature of current approaches to detect in-field anomalies, applied mostly to aerial imagery and near-ground sensors, is sensitive to noise (producing a salt and pepper effect) and makes it difficult to account for contextual information Chen et al. (2012). The use of kernel filters, or moving windows, enables pixels contextual information to be considered (Tewkesbury et al., 2015). For these approaches, often hard thresholds are applied to spectral data in a plot based on statistical metrics retrieved from the distribution of the data within a moving window. McCann et al. (2017) mapped local anomalies based on the number of Median Absolute Deviations (MADS) for a given moving window around a centre pixel. Although this demonstrated promising results, the accuracy obtained varied highly depending on the window size, growth stage and number of MADS chosen (McCann et al., 2017).

Rather than using variable kernels to define anomalous pixels, object-based image analysis (OBIA) offers an opportunity to use the agricultural plot as a fixed spatial unit of analysis. It eliminates the window size variable and is especially relevant for in-field anomaly detection, given the fact that agricultural management decisions are usually made on a per-field basis (Belgiu and Csillik, 2018; Long et al., 2013). OBIA is, however, preferred only if the objects of interest (i.e. agricultural fields) are significantly larger than the pixels of the image (Blaschke, 2010; Gilbertson and van Niekerk, 2017). This, therefore, excludes the use of broad spatial resolution sensors such as MODIS and SPOT-VGT for in-field anomaly detection and restricts the use of Landsat when monitoring plots smaller than 4 ha, as there would not be a sufficient number of pixels to carry out a robust analysis. Sentinel-2 imagery, with a 10–20 m spatial resolution and a revisit time of 5 days, provides an opportunity to explore the use of freely available EO data for conducting OBIA-based crop monitoring in small to medium size crop plots.

Thresholding spectral data to determine whether pixels are anomalous or not is also challenging and current research is still limited. This is because each crop plot has its particular characteristics (e.g. soil properties, plant species, phenological stage, weather conditions, or management practices) that need to be accounted for independently. Several studies have developed methods that use ground truth data to train the anomaly detection models or tune the value of the threshold point to produce higher accuracies (e.g. Liang et al., 2021; Kanjir et al., 2018; McCann et al., 2017; Mouret et al., 2021). However, few authors, such as Thomas et al. (2018) that developed a histogram-based technique to detect mangrove forest changes, have developed automatic thresholding techniques for anomaly detection. With constantly improving technology in terms of the sensors, satellite EO offers the potential to develop transferable, scalable, and low-cost PA solutions to detect in-field crop anomalies and implement corrective actions that maximise the production along the crop cycle. It requires methods that automatically tune the threshold values for each crop plot, considering its particular biophysical conditions.

This research presents a novel approach for the detection of in-field crop anomalies over space and time using medium and high-resolution EO-derived products. The Earth Observation-based Anomaly Detection (EOAD) approach implements a simple histogram analysis technique for delineating potentially anomalous pixels. This was tested over rice plots in the Ibague Plateau, Colombia, with comparisons being made with field observations of anomalous areas and final yield data. We also tested the ability of the EOAD to forecast low-performance fields at early growth stages to prioritise efforts to optimise the overall productivity in the whole agricultural system.

2. Materials and methods

2.1. Study area

The demonstration area is located within the Ibague plateau plain in the Central Andes, Colombia, at 4.3 °N, 75.0° W (Fig. 1). The altitude varies between 704 and 934 meters above sea level and the climate is semi-humid, with an average temperature of 23.2° C and annual average precipitation of 1690 mm (Instituto de Hidrología Meteorología y Estudios Ambientales de Colombia, 2020).

The most important agricultural production system in the area is irrigated rice (*Oryza sativa*). The rice cycle duration ranges between 115 and 130 days after the emergence date (DAE), and due to the equatorial climatic conditions, the cereal is produced throughout the year, for which the crop calendar among neighbouring fields can be different.

The period of rice growth can be divided into three agronomic phases: 1) vegetative, 2) reproductive, and 3) ripening/grain filling (Kuenzer and Knauer, 2013; Moldenhauer et al., 2013). The classification of the sub-phases within these 3 main stages varies among farming systems. Growers in the Ibague Plateau sub-divide the vegetative phase of rice into three further substages: i) Germination, ii) seedling emergence, iii) tillering and a ripening/grain filling (See Fig. 2). The plot age is counted from the field date of emergence, which is defined as the date when 80% of the plants have emerged.

Rice fields are irrigated using a contour-levee technique. Under this irrigation technique, the water layer depth is dynamically changing over space and time, leading to a heterogeneous development of rice plants and weeds along the field (Okada and Lopez-Galvis, 2018). When dry patches are identified, the water flow is fixed, so the plants grow at the expected rate.

2.2. Datasets and Image processing

2.2.1. Field Observations

Field observations were made over a 100 m regular grid between December 2019 and February 2020. A total of 36 reference points were recorded in 8 plots using the QField mobile app Version 1.2 on a mobile phone. For each point, the coordinates, the presence/absence of
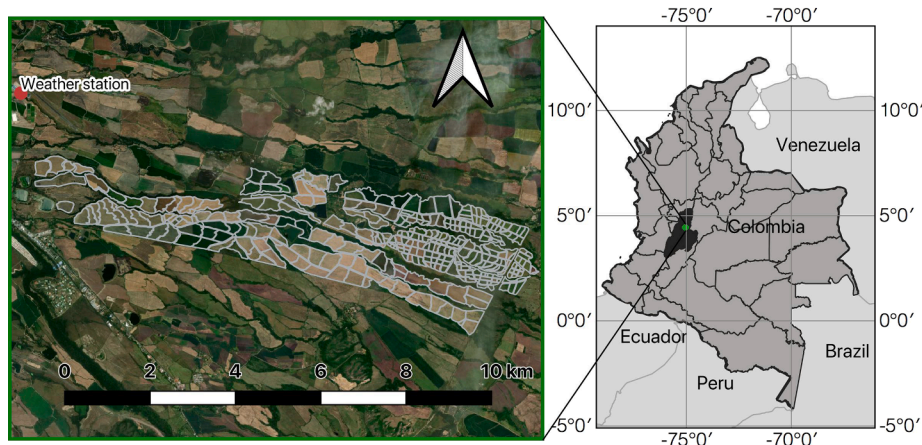
Fig. 1. Map showing the location of the Ibague plateau study site, Colombia.
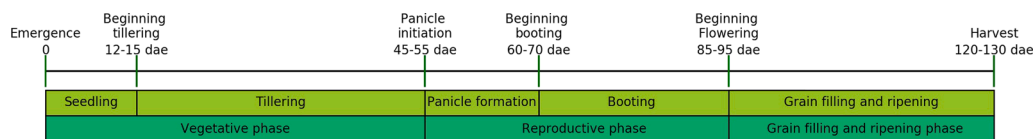

Fig. 2. Rice phenology at the Ibague Plateau.

anomalies, the type of anomaly (When the observation was considered anomalous) and a picture were registered. The identification of the presence/non-presence of anomalies in each point was performed visually by the farm agronomists, based on their expertise and crop knowledge.

To account for GPS accuracy, a 10 m radius buffer was applied around each field data collection point. Field boundaries were manually digitised using PlanetScope imagery and ground control points. Although this was a highly manual approach, published methods demonstrate the potential for automatically delineating both regular and irregular shaped agricultural fields using medium resolution EO imagery (Robb et al., 2020). A negative 10 m buffer was applied over the crop plot boundaries to reduce edge effects and potential image alignment artefacts.

2.2.2. EO Imagery

Satellite optical data were acquired over the study site between January 2018 and February 2020 (Fig. 3). These datasets were selected to test the performance of the anomaly detection technique using widely used commercial (PlanetScope) and non-commercial (Sentinel-2) EO imagery.

For this study, 47 Sentinel-2 images were downloaded via Google Cloud Public Dataset and 15 Planet imagery were accessed through the Planet Explorer browser (Fig. 3).

The Sentinel-2 mission comprises a constellation of two polar-orbiting satellites placed in the same sun-synchronous orbit. It provides 10 days revisit at the equator with one satellite and 5 days with 2

satellites (ESA, 2013). Each Sentinel-2 satellite carries the Multi-Spectral Instrument (MSI), which measures the Earth's reflected radiance in 13 spectral bands (See Fig. 4). The Sentinel-2 Level-1C products are top-of-atmosphere reflectance ortho-images in UTM/WGS84 projection. They are resampled with a constant Ground Sampling Distance (GSD) of 10, 20, and 60 m, depending on the native resolution of each spectral band (ESA, 2013).

The Sentinel-2 L1C products were processed to surface reflectance and terrain corrected using the 6S radiative transfer model in the Atmospheric and Radiometric Correction of Satellite Imagery (ARCSI) software (Bunting et al., 2018). All image bands were sampled to 10 × 10 m resolution and clouds and shadows were masked through using an extra-trees classifier.

The commercial PlanetScope constellation consists of individual satellites (Doves) that follow a Sun-Synchronous orbit and are able to acquire daily images from the entire Earth's surface (Lemajic Blanka et al., 2018; Wicaksono and Lazuardi, 2018). Each PlanetScope CubeSat has a four-band frame imager with a split-frame Visible + Near-Infrared filter, resampled with an approximate GSD of 3.7 m at nadir (Planet Labs, 2019).

PlanetScope 3B level images, acquired between January 2019 and February 2020, are delivered as orthorectified, surface reflectance image products (Planet Labs, 2019) and no additional pre-processing operations were applied to them.

The resulting Analysis Ready Data (ARD) was used to calculate a suite of vegetation indices (VIs) demonstrated in previous studies to be sensitive to a variety of crop properties (See Table 1). The selected
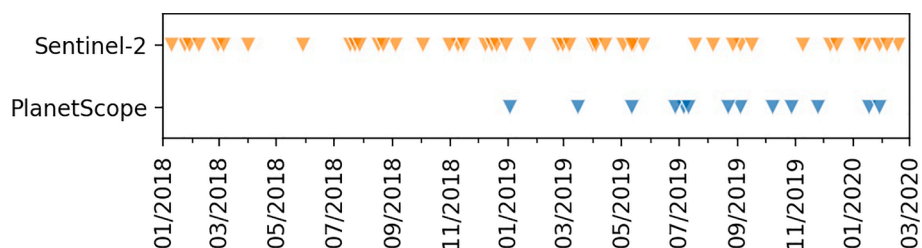

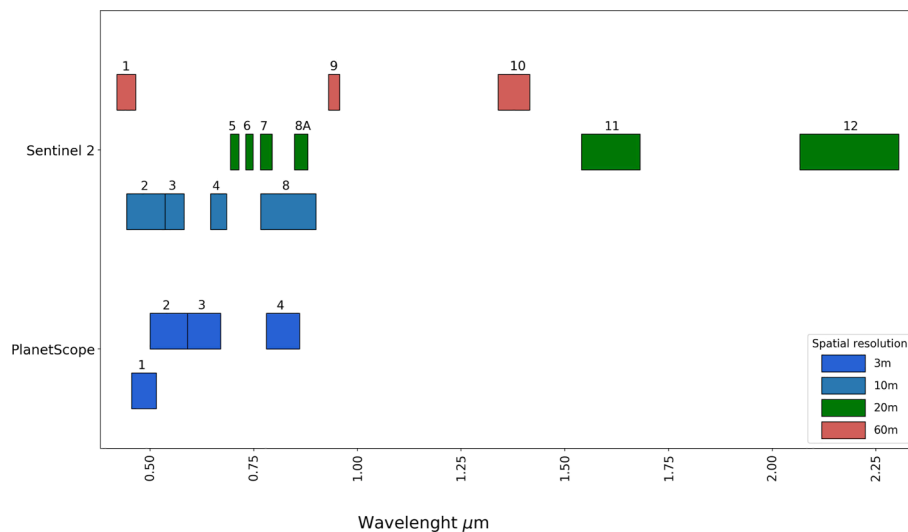**Fig. 3.** Acquisition dates of the PlanetScope and Sentinel-2 scenes.

Fig. 4. Planet Scope and Sentinel-2 spectral wavelengths differentiated by spatial resolution.

indices have shown to be good indicators of two main categories of crop biophysical properties: 1) Photosynthetic Pigments (PP) and 2) Vegetation and soil Water Content (VWC). Due to its relatively limited spectral capabilities, not all VIs were able to be calculated using the PlanetScope imagery (five in total, compared to 24 for Sentinel-2). Sentinel-2 has more than one Near-infrared (NIR) and red-edge channels; therefore, all possible combinations of these VIs were considered (e.g. Normalised Difference Vegetation Index was calculated for Sentinel-2 twice: The first using band 8 and the second using band 8a).

2.2.3. Yield measurements

The yield was measured by a sensor mounted on the rice combine harvester that recorded an estimated wet grain yield (T/ha) per linear meter. Yield data was interpolated into raster surfaces using inverse distance weighting and resampled to match the EO derived products using a bilinear interpolation. The yield values for all the plots were normalised between 0 and 1 to minimise the production variability among plots due to different management conditions.

2.3. The EO-based plot-level Anomaly Detection (EOAD) technique

The Optical vegetation indices were used as input for the EO-based plot-level Anomaly Detection (EOAD) method. The anomaly surfaces obtained were then compared with the ground data to detect the method accuracy and the impact of the predicted anomalies over the yield. The methodological workflow is presented in Fig. 6.

2.3.1. Histogram analysis

The EOAD technique is based on thresholding the histogram of EO data (i.e. VI values) within a crop plot. The python algorithm to implement the EOAD method can be found at Castillo-Villamor et al. (2021). Thresholds are designed to classify pixels into one of three classes: 1) high-anomalous, 2) low-anomalous and 3) non-anomalous. There are two key assumptions that EOAD is based on: i) VI values for non-anomalous pixels will be normally distributed in a crop plot, and ii) pixel values that deviate from this normal distribution are considered anomalous (i.e. significantly high or significantly low values). The thresholding process used by EOAD is illustrated in Fig. 5. Here, pixels are excluded by iteratively removing the tail bins of the VI histogram (per plot) until normality is achieved. The degree of normality is based on measures of kurtosis and skewness, where the iteration that produced the lowest kurtosis and skewness represents the most normal distribution. At this point, the upper and lower bin values are extracted, representing corresponding thresholds for determining whether a pixel is

considered high-anomalous or low-anomalous, the rest remaining as non-anomalous. This approach allows considering the inherent variability of the properties of the plot, independently of the variability that may occur between parcels as a consequence of different management practices. The bin width (BW) is defined independently for each plot following Freedman and Diaconis (Freedman and Diaconis (1981)) using the interquartile range (IQR), where n is the number of available values (See Eq. 1).

$$BW = \left(2 \times IQR \times n^{-1/3}\right) \tag{1}$$

2.3.2. Accuracy assessment

The EOAD approach was initially validated against field observations of anomalies to determine which VI products could accurately map anomalies. Secondarily, statistical comparisons were drawn with yield data to determine EOAD's potential for directly informing agricultural practices that lead to increases in yield. A summary of these analyses is provided in Fig. 6.

EOAD was applied to all crop plots at the study site using all available VIs outlined in Table 1. A set of field validation points were used to assess the accuracy of the EO-based anomaly detection technique for identifying true anomalies observed in the field. The 10 m buffer area associated with each ground point was intersected with the anomaly presence/absence classified products where the corresponding EO and field collection dates were within 8 days. For the studied rice plots, the 36 reference points were found in four (4) Sentinel-2 and four (4) PlanetScope images within ±8 days, resulting in 78 and 72 observations, respectively. For each observation, the EO-derived anomaly status was compared against the anomaly status recorded in the field using a confusion matrix, thereby summarising the number of true positives (TP), false positives (FP), false negatives (FN) and true negatives (TN).

Two standard metrics were derived from the confusion matrix (See Table 2): The overall accuracy (OA) and the true skill statistic (TSS). The overall accuracy represents the proportion of correctly predicted sites. It is defined as the ratio between the correctly classified points to the total number of points (Sokolova et al., 2006; Tharwat, 2021). The TSS, also known as the Hanssen-Kuipers discriminant, compares the number of correct predictions, minus those attributable to random guessing, to a hypothetical set of perfect predictions. The TSS is used to correct the model's overall accuracy by the accuracy expected to occur by chance (Allouche et al., 2006).

2.3.3. Period with lower presence of climatic extreme events

To control for variations caused by climate and prevailing weather,

Table 1
Multi-spectral vegetation indices evaluated.

Index	Formula	Convention/bands	
		Sentinel-2	PlanetScope
NDVI	$\dfrac{\rho_{nir} - \rho_{red}}{\rho_{nir} + \rho_{red}}$	NDVI_b8 (ρ_{833}, ρ_{665}) NDVI_b8A (ρ_{865}, ρ_{665})	NDVI (ρ_{820}, ρ_{630})
SAVI	$\dfrac{(1+L)(\rho_{nir} - \rho_{red})}{\rho_{nir} + \rho_{red} + L}$	SAVI_b8 (ρ_{833}, ρ_{665}) SAVI_b8A (ρ_{865}, ρ_{665})	SAVI (ρ_{820}, ρ_{630})
EVI	$G \dfrac{\rho_{nir} - \rho_{red}}{\rho_{nir} + C_1\rho_{red} - C_2\rho_{blue} + L}$	EVI_b8 (ρ_{833}, ρ_{665}) EVI_b8A (ρ_{865}, ρ_{560})	EVI (ρ_{820}, ρ_{630})
CIg	$\dfrac{\rho_{nir}}{\rho_{green}} - 1$	CIg_b8 (ρ_{833}, ρ_{560}) CIg_b8A (ρ_{865}, ρ_{560})	CIg (ρ_{820}, ρ_{545})
CIre	$\dfrac{\rho\_nir}{\rho\_red-edge} - 1$	CIre_b8_5 (ρ_{833}, ρ_{704}) CIre_b8_6 (ρ_{833}, ρ_{740}) CIre_b8_7 (ρ_{833}, ρ_{783}) CIre_b8A_5 (ρ_{865}, ρ_{704}) CIre_b8A_6 (ρ_{865}, ρ_{740}) CIre_b8A_7 (ρ_{865}, ρ_{783})	
GNDVI	$\dfrac{\rho_{nir} - \rho_{green}}{\rho_{nir} + \rho_{green}}$	GNDVI_b8 (ρ_{833}, ρ_{560}) GNDVI_b8A (ρ_{865}, ρ_{560})	GNDVI (ρ_{820}, ρ_{545})
RENDVI	$\dfrac{\rho_{nir} - \rho_{red-edge}}{\rho_{nir} + \rho_{red-edge}}$	RENDVI_b8_5 (ρ_{833}, ρ_{704}) RENDVI_b8_6 (ρ_{833}, ρ_{740}) RENDVI_b8_7 (ρ_{833}, ρ_{783}) RENDVI_b8A_5 (ρ_{865}, ρ_{704}) RENDVI_b8A_6 (ρ_{865}, ρ_{740}) RENDVI_b8A_7 (ρ_{865}, ρ_{783})	
NDII	$\dfrac{\rho_{nir} - \rho_{swir}}{\rho_{nir} + \rho_{swir}}$	NDII_b8_11 (ρ_{833}, ρ_{1610}) NDII_b8_12 (ρ_{833}, ρ_{2186}) NDII_b8A_11 (ρ_{865}, ρ_{1610}) NDII_b8A_12 (ρ_{865}, ρ_{2186})	

For SAVI, the canopy background adjustment constant L accounts for differential near-infrared extinction through the canopy. For EVI, L is a soil adjustment factor, G is a gain factor, set to 2.5, and C1 and C2 are coefficients that describe the use of the blue band to correct the red channel for aerosol scattering (Set to 6 and 7.5, respectively)

satellite data analysed were acquired during a period that was not considered extremely wet or dry conditions defined by the Standardised Precipitation Index (SPI), where SPI was between −1.5 and 1.5 (McKee et al., 1993). SPI was calculated using historical rainfall records between 1980–2010 from the meteorological station of the Perales Airport (4.4241 °N, 75.1394° W). Hereafter, we will refer to this as the typical precipitation period. It is used to determine the time-lapse to assess the impact of the predicted anomalies over the yield.

2.3.4. Impact of anomalies at different crop stages over yield

Those Sentinel-2 VIs with overall accuracy scores above 70% and TSS values greater than 0.5 were analysed further to determine whether EOAD-observed anomalies were related to crop yield. Firstly, the anomaly-predicted surfaces derived from each product were compared with the final yield to identify if such anomalies at distinct growth stages impacted the final production.

The yield for anomalous and non-anomalous pixels at each of the five growth stages was compared using an independent two-sample t-test when the two samples variances were equal and a Welch-Satterthwaite test when the variances were unequal. The analysis was performed over a sample extracted from all the pixels falling within 13 plots, sown with four rice varieties during the typical precipitation period.

2.3.5. Early detection of underperforming plots

The percentage of the anomalous area within each plot was used as one predictor of low-performing plots in the rice production system. If this relationship proved to be true, it might help prioritise those fields that require more immediate attention and therefore optimise the overall productivity in the agricultural system.

First, a set of thresholds were established to classify the farm historical yield into high and low. The thresholds were chosen in terms of the different number of standard deviations away from the farm yield mean, as presented in Table 3.

For each of these thresholds, we used two sets of variables as predictors of high and low yield plots at each of the single growth stages:

- Set of variables A: Mean VI per plot, rice cultivar and emergence month.
- Set of variables B: Mean VI per plot, percentage of the anomalous area within the field, rice cultivar and emergence month.

To reduce the problems that imbalanced data can create in the classification, the training data was balanced for high/low yields at each threshold by random oversampling (Japkowicz and Stephen, 2002). Balancing was done independently for each VI and threshold at the different growth stages.

The tree-based pipeline optimization tool - TPOT, (Le et al., 2020) was used to define the machine learning classifier to be trained. The TPOT classifier class (TPOTClasifier) was used over the two groups of
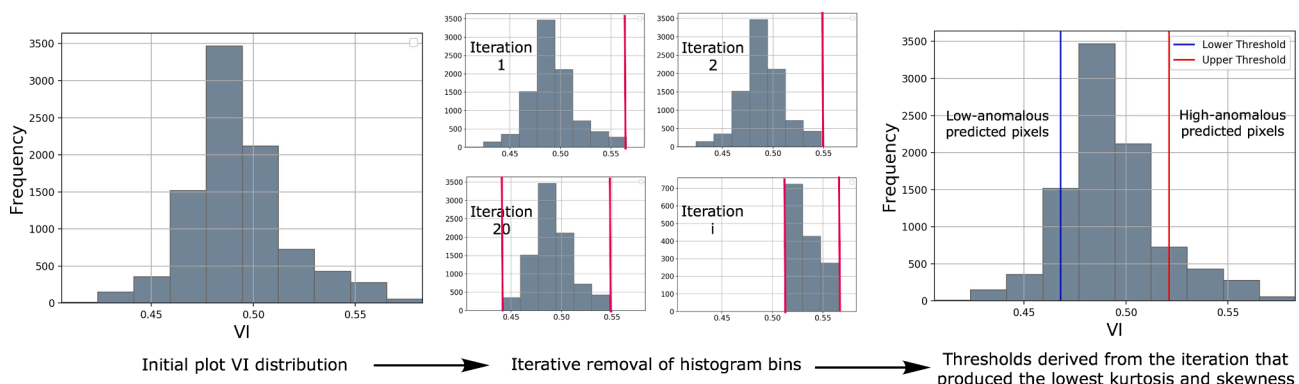

Fig. 5. Extraction of thresholds using the histogram analysis approach.
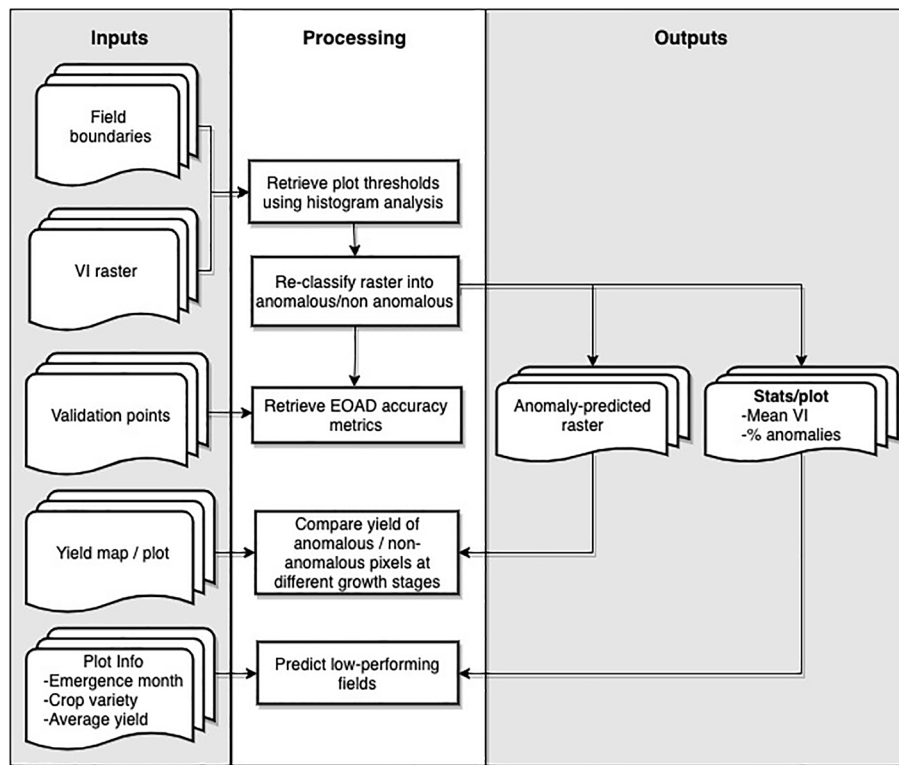
Fig. 6. Flowchart describing the processes involved in the anomaly detection method and assessment.

Table 2
Performance metrics derived from the confusion matrix.

Metric	Formula
Overall accuracy (OA)	$\dfrac{TP + TN}{TP + TN + FP + FN}$
TSS	$\dfrac{(TP \times TN) - (FP \times FN)}{(TP + FN) \times (FP + TN)}$

Table 3
Yield thresholds.

Threshold	1	2	3	4
Value	$\overline{X}$	$0.5\,\sigma$	σ	$1.5\,\sigma$

predictors using the NDVI_b8 data during the seedling and booting stages with default hyperparameters, with the exception being the following:

- Number of generations: 50;
- Population size: 50;
- Population size: 50;
- Number of cross-validation folds (CV): 5.

The resulting best model was trained for all VIs using the data available at each phenological stage in such a way that 75% was being used as the training set while the remaining 25% was used as the test set.

K-fold cross-validation for the area under the ROC curve (Bradley, 1997; Hanley and McNeil, 1982) was used to assess the model performance for each threshold and VI at each growth stage. The mean AUC and the AUC standard deviation were retrieved for each of the 5 folds.

3. Results

A worked example of how the EOAD technique automatically splits

the VIs histogram data into high-anomalous, low-anomalous and non-anomalous pixels is given in Fig. 7. Among the anomalies identified in the field, over 87% were due to two main factors: (1) water shortages and (2) low plant density. In terms of growth, 75% of field-observed anomalies were registered during the tillering stage, between 33 and 44 DAE. The remaining 25% anomalous points were identified during the booting stage (70 days). Where EOAD was able to accurately detect true-anomalous points, 56% registered as having lower plant density than the plot average, and over 37% exhibited a shortage of water. All areas identified as having a water shortage also presented lower plant development in comparison with the other plants in the plot.

3.1. Accuracy differences among vegetation indices

Fig. 8 presents the values of the metrics used to assess the EOAD accuracy for different VIs. Overall, the VIs that showed the highest accuracies (>70%) in terms of correctly identifying anomalous points in a plot, were related to normalised difference indices that use the NIR bands, i.e. NDVI, SAVI and GNDVI. The accuracy of the NIR-based VIs seemed to remain consistent between Sentinel-2 and PlanetScope, demonstrating their relative robustness in terms of accurately representing anomalous areas in a crop plot. Interestingly, there was no significant difference in the accuracy obtained using the NDVI when calculated by either Sentinel-2 band 8 (10 m), Sentinel-2 band 8a (20 m) or PlanetScope (3 m), suggesting that spatial scale is not a controlling factor, at least for this particular VI.

For Sentinel-2, the highest accuracies evidenced in Fig. 8 (overall accuracies above 70% and TSS greater than 0.5) were reached using normalised difference indices estimated with the band 8 (i.e. SAVI_b8, GNDVI_b8, reNDVI_b8_5 and NDVI_b8). Among the VIs that employed the red-edge channels ($n = 3$), only those where the red-edge band 5 was used, produced accuracies above 70%. Similar trends are presented in terms of TSS, where those indices that included the red-edge band 5 showed improved accuracy in comparison with red-edge bands 6 and 7. Among the red-edge indices considered, the reNDVI always showed
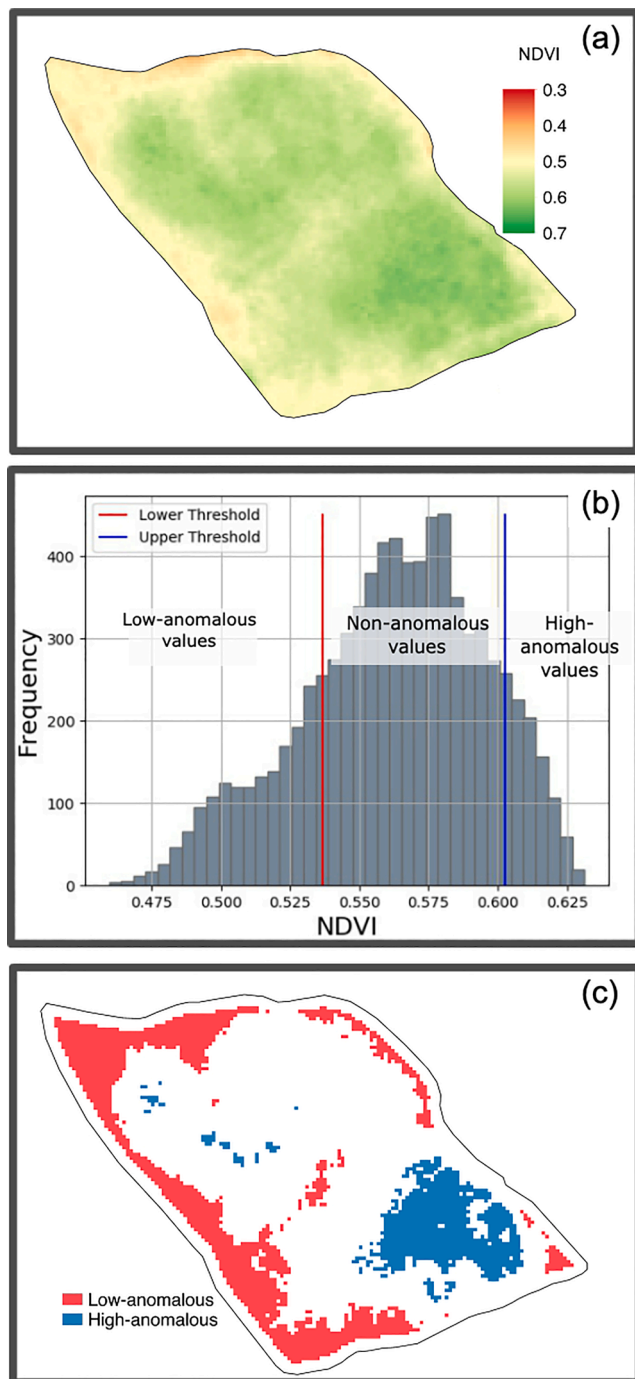
Fig. 7. Example of the histogram analysis performed over one rice field. (a) The NDVI raster, (b) thresholds that produced the lowest kurtosis and skewness, (c) anomaly-predicted surface.

significant higher accuracies in comparison with CIre. In general, the lowest accuracies recorded were obtained with VIs that included the red-edge bands 6 and 7. Similarly to Sentinel-2, the NDVI estimated with PlanetScope images showed higher accuracy in comparison with other normalised indices (i.e. CIg, and GNDVI). However, unlike the Sentinel-2 derived indices, the use of EVI showed increased accuracy and the GNVI index produced one of the lowest accuracies. For these indices, recorded true-positives were exclusively related to low-anomalies. As such, analysis from this point only relates to detected low-anomalies.

3.2. Period with lower presence of climatic extreme events

The typical precipitation period was set between January 2018 and July 2019 to avoid the effects that the high SPI in November 2017 could have on the plants. Fig. 9 presents the SPI values estimated from January 2016 until March 2020 and the thresholds (SPI=± 1.5) that determine the typical rainfall period.

3.3. Impact of anomalies at different crop stages over yield

Fig. 10 shows the normalised yield obtained for anomalous and non-anomalous pixels and the t-test values of the comparisons of these 2 groups for the Sentinel-2 VIs with overall accuracy scores above 70% and TSS values greater than 0.5. Among the different growth stages, the presence of anomalies during the booting stage using normalised difference indices in the visible and NIR were significantly associated with final yield ($\alpha = 0.05$). In general, those pixels found anomalous during the booting stage using the GNDVI_b8, reNDVI_b8_5, and NDVI_b8 indices tended to produce significantly lower yields at the harvest.

The shortwave infrared-based index NDII calculated with the band 8 showed significant differences ($\alpha = 0.005$ and $\alpha = 0.05$) in yield between anomalous and non-anomalous areas occurring during the seedling stage. Fig. 11 shows the normalised yield obtained for anomalous and non-anomalous pixels and the t-test values of the comparisons of these 2 groups for two band combinations of Sentinel-2 NDII indices. NDII is an indicator of water content and the region of 2190 nm (Band 12), particularly, has shown to be more sensitive to soil moisture than band 11 at 1640 nm (Wang et al., 2008). Yields for anomalous pixels (lower values) found with the NDII (band 8) tended to be higher. The NDII values of those pixels were mostly positive and associated with areas with a higher soil and plant water content, based on the visual observations in the field.

3.4. Early detection of anomalous plots

The histogram of the historical average plot yields in the farm, as well as the four thresholds defined to classify plots into high and low performing, are presented in Fig. 12. The farm yield values did not show evidence of non-normality after performing a Shapiro–Wilk test ($\alpha = 0.05$, W $= 0.99$, p-value $= 0.103$).

The Gradient Boost (GB) classifier was selected as the most suitable model to predict high and low performing plots during the seedling and booting stages using TPOT over the NDVI_b8 products. The cross-validated mean AUC values of the GB classifier for all the VIs at different growth stages are presented in Fig. 13.

In general, the classifier performance improved as the yield thresholds moved away from the mean. The addition of the percentage of the anomalous area within the plot improved the performance of the model for all the thresholds above the yield mean. In both sets of variables, the model fit to the booting and ripening data showed cross-validated mean AUC values above 90% and above 80% when fit to the seedling and tillering data for the thresholds above the yield mean. Despite the high performance at predicting high/low yield plots at the ripening stage, it is too late to implement actions that optimise crop productivity.

The increased performance of the model fit to the booting and ripening data is also evidenced in the variability of the cross-validated mean AUC values. Fig. 14 shows that the mean AUC values variability for the model, fit over the set of variables B, is lower at booting and ripening stages. In contrast, the panicle formation presents not only the lowest CV mean AUC values but also the larger standard deviation of these values.

4. Discussion

The proposed Earth Observation derived Anomaly Detection (EOAD) method was able to identify and map crop anomalies with accuracy
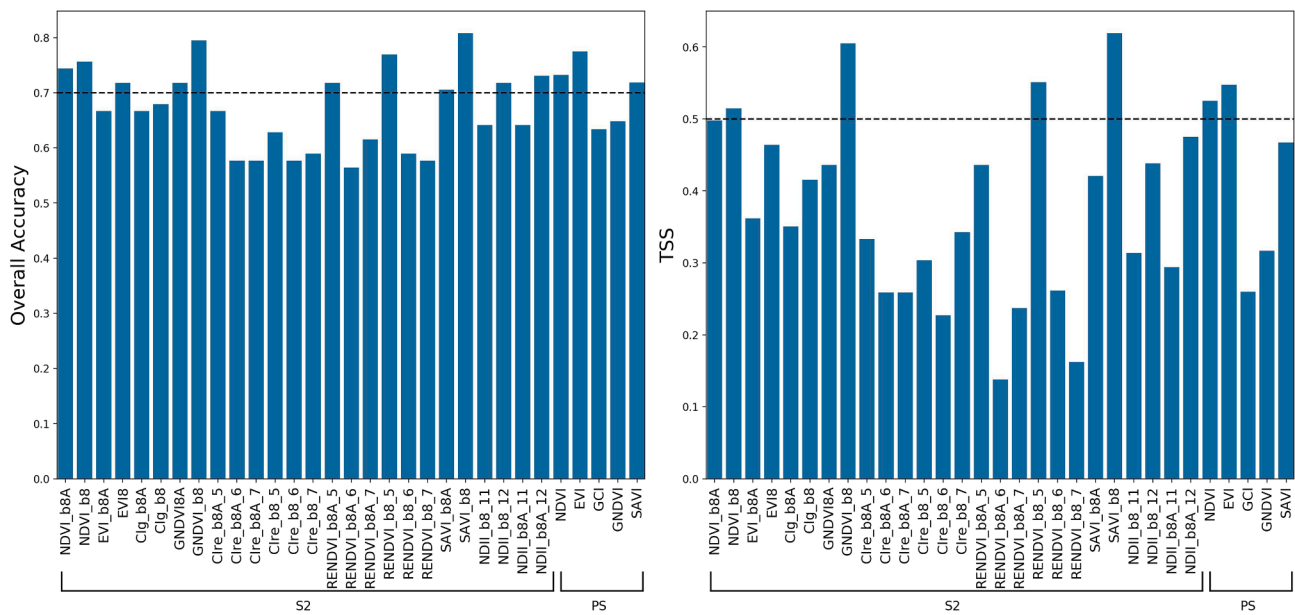
Fig. 8. Anomaly detection accuracy metrics obtained with the optical vegetation indices.
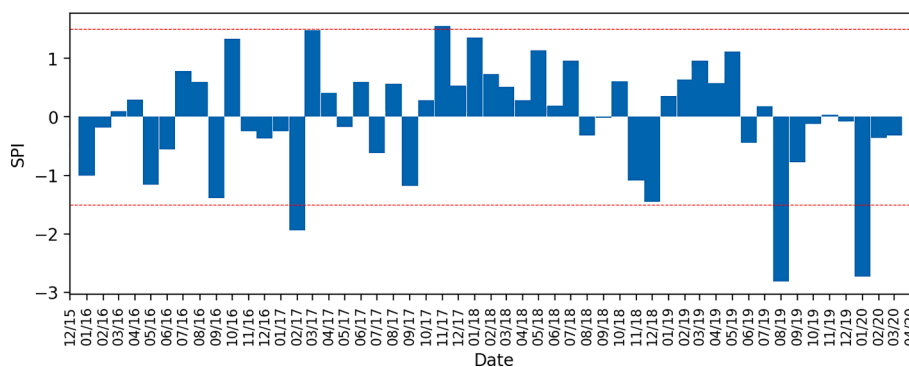

Fig. 9. SPI values from January 2016 until March 2020.

scores up to 80% comparing favourably with other anomaly detection approaches reporting accuracies of 50–70% (e.g. McCann et al., 2017). EOAD is based on a simple automatic thresholding approach applied to the distribution of VI values within a crop plot. Its simplicity and reliance on the basic statistics of a field/plot's pixels mean that it can be transferred to any VI or, indeed, any geographically continuous data, e. g. point cloud metrics, gridded temperature etc.

This automated approach offers procedural advantages over other approaches, such as McCann et al. (2017) that detected anomalies by applying manually set thresholds to Median Absolute Deviation (MAD) values calculated over a moving window. Furthermore, because the McCann et al. (2017) employs a moving window, thereby taking advantage of the relatively high spatial resolution aerial or drone imagery to which it was applied, the size of the anomalous area detected is limited to the size of the kernel used, i.e. areas smaller than the kernel will be missed, whereas EOAD can detect anomalous areas at the pixel level making it better suited to relatively course satellite EO data.

The EOAD approach was successful in detecting (overall accuracy >70%) anomalous pixels using both Sentinel-2 and PlanetScope imagery. This consistency demonstrates the potential for applying the approach to a range of broadband EO systems. A major drawback of optical EO imagery is the dependence on cloud-free conditions, but the consistency in performance over the two sensors investigated offers the potential to detect anomalies in relatively large (> 4 ha) crop plots, using different systems, e.g. Sentinel-2 and Landsat, meaning a greater

frequency of revisit, a higher chance of making cloud-free observations and increases the monitoring frequency throughout the growing cycle. Future work should implement EOAD to Landsat imagery to demonstrate its transferability to this widely used source and exploit its rich archive of data.

Intelligent management of water throughout the crop cycle is essential for overall profitability, management of diseases, nutrient management and development of rice plants (Henry et al., 2018). Under the contour-levee irrigation scheme, the level of homogeneity in water distribution along the plot is defined when the "irrigator" sets the levees breaks during the field preparation (Okada and Lopez-Galvis, 2018). In later crop stages, the lack of adequate water supply is reflected not only in the plant growth but also in the activation of products applied, such as fertilisers or herbicides (Henry et al., 2018; Vories et al., 2017).

The sooner in-field anomalies are identified and fixed; the more homogeneous the final yield and grain quality will be (Marchesi et al., 2010). The EOAD approach can be used to detect these types of anomalies, particularly, the NDII_b8_12 index showed to detect anomalies related to soil moisture in the early stages of the crop and apply irrigation to aid emergence (Takeda et al., 2019). Similarly, the approach can be used to detect patches with low plant density due to other factors such as seed quality and sowing/soil heterogeneity in order to re-sow the seeds (Jarrod Hardke et al., 2018). In the present study, anomalous-detected areas were targeted by farm staff to detect dry patches and fix the water supply or identify the areas with low plant density for site-
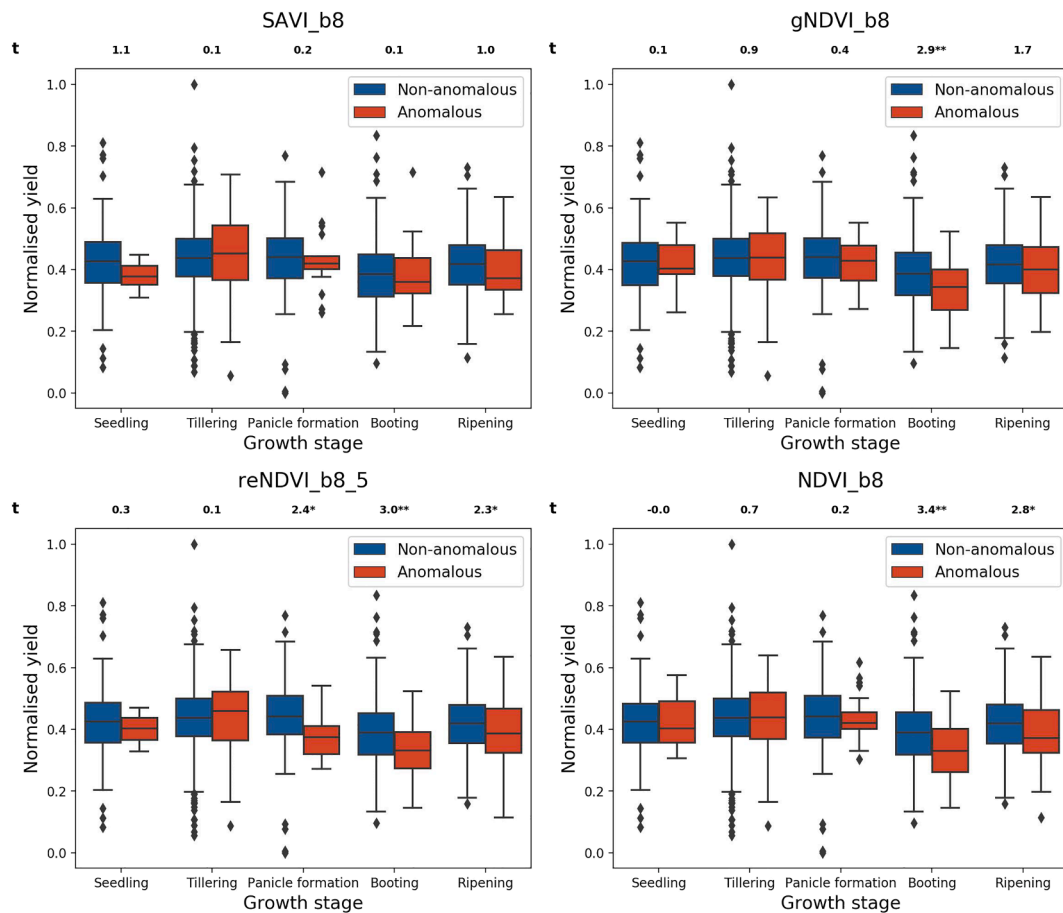
Fig. 10. Box plots of yield obtained for anomalous and non-anomalous pixels values at different growth stages (VIs that showed the highest accuracy and TSS). The t-test values correspond to each pairwise comparison between pixels predicted as non-anomalous (blue box-plot) and those predicted as anomalous (red box-plots) ** Significant at $\alpha = 0.005$; * Significant at $\alpha = 0.005$.
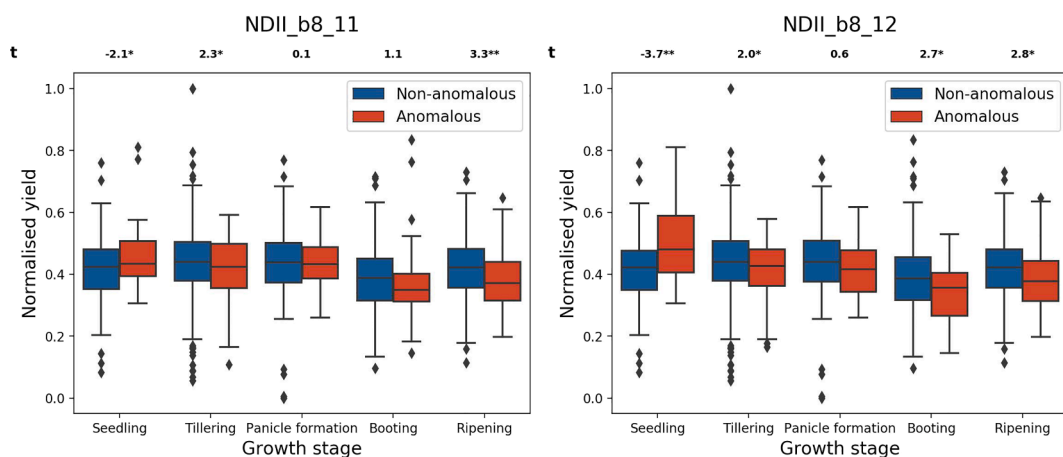

Fig. 11. Box plots of yield obtained for anomalous and non-anomalous pixels values at different growth stages using the NDII (band 8). The t-test values correspond to each pairwise comparison between pixels predicted as non-anomalous (blue box-plot) and those predicted as anomalous (red box-plots). ** Significant at $\alpha=0.005$; * Significant at $\alpha =0.005$.

located re-sowing.

Due to the constant and careful monitoring activities performed by the farm staff daily, the proportion of anomalies registered in the field were small in comparison to the field area (<3%). Nevertheless, in circumstances where the amount of change increases, the tailed histogram shape makes it more challenging to find an optimal threshold. For example, one rice plot, which was not considered in the field sampling in

this study, was unevenly treated with Nitrogen fertiliser (by aeroplane), manifesting itself in a left-tailed histogram of PlanetScope-derived NDVI values (Fig. 15). Although this scenario did not actually occur in any field sampled, and it might not produce an optimum threshold, it gives insights about how the technique can still produce sensible responses under the presence of larger anomalous areas. This information alerts the farmer about the presence of potentially anomalous zones. Further
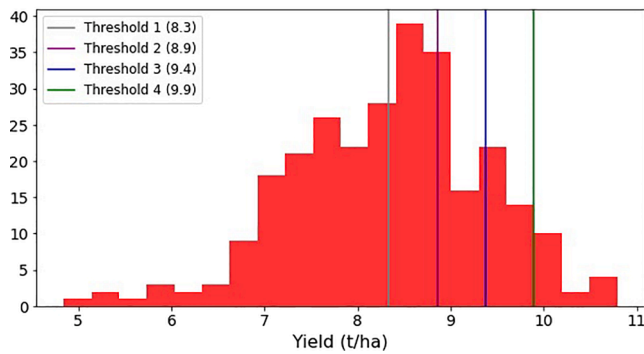
Fig. 12. Histogram of farm average yield values per plot and thresholds used to classify the fields into high and low performing.

research has to be done to establish a more robust relationship between the extent of the anomalous area and the accuracy of the thresholds detected.

Although the EOAD approach was only demonstrated for rice crops, the approach is based on the variability in reflectance as an indicator of biophysical properties of the crops, particularly canopy density. This is

not unique to rice crops, and therefore there is clear potential to be applied to different crop types and different agricultural systems. It is likely that where other crops are considered, different physical characteristics of the crop would be more important in determining whether an area of a field is considered anomalous or not. The intention of EOAD is not to provide a definitive prediction or estimate of biophysical properties, but its simplicity and reliance on freely available EO data means that it can be used as a convenient alternative for systematic anomaly screening that is fundamental in crop management, i.e. decision-makers can focus attention towards areas identified as anomalous and perform site-specific practices based on their expertise and knowledge about the crop and its context. Indeed, the EOAD approach as a whole tried to deviate from previous PA approaches by providing broad indications to the farmer for further inspection on the ground, rather than attempting to provide a definitive prediction of, for instance, plant Nitrogen content or final yield. This is especially important in relatively resource-limited regions of the world where farm data monitoring networks that supply spatial and temporal information on the biophysical properties of agricultural systems are prohibitively expensive.

For Sentinel-2, EOAD performed best when VIs were used that relate to LAI and vegetation coverage, namely, the SAVI_b8 and GNDVI_b8 indices (Overall accuracy 80% and TSS > 0.6). Although EOAD can detect both high and low anomalies, true positive matches with field
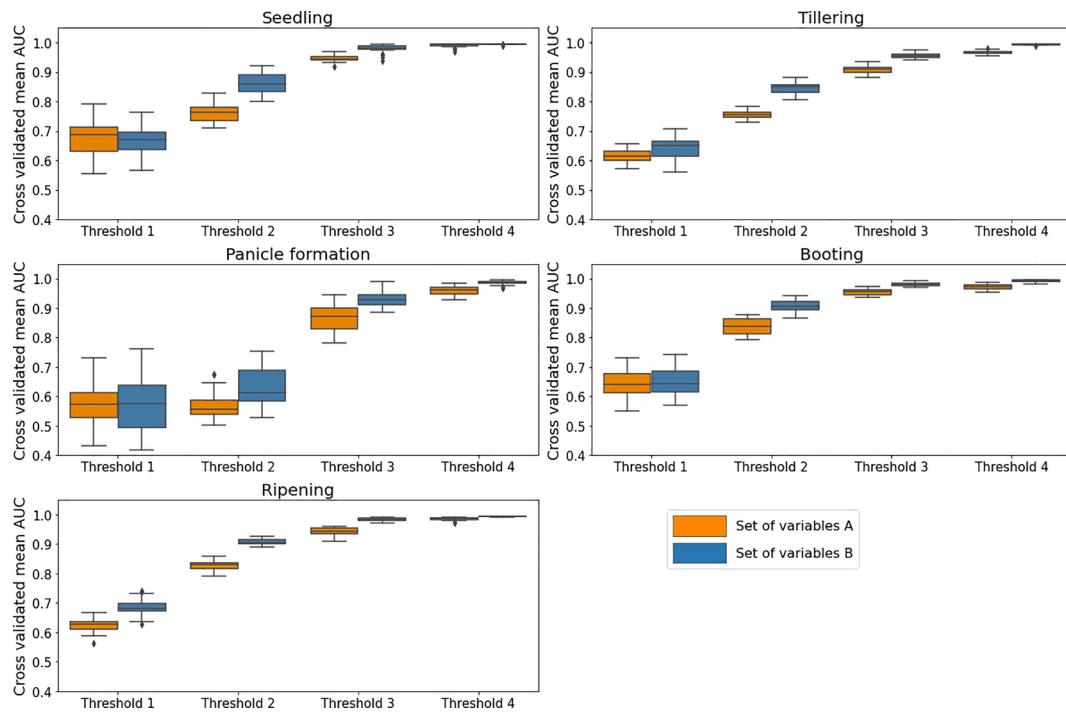

Fig. 13. Cross validated mean AUC values of the GB classifier for all the VIs at different growths stages using the two sets of variables.
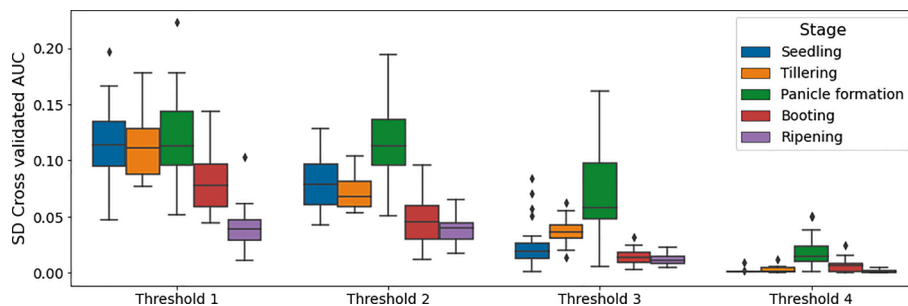

Fig. 14. Standard deviation of cross-validated AUC values of the GB classifier fit to the set of variables B at different crop growth stages for the VIs presented in Table 1.
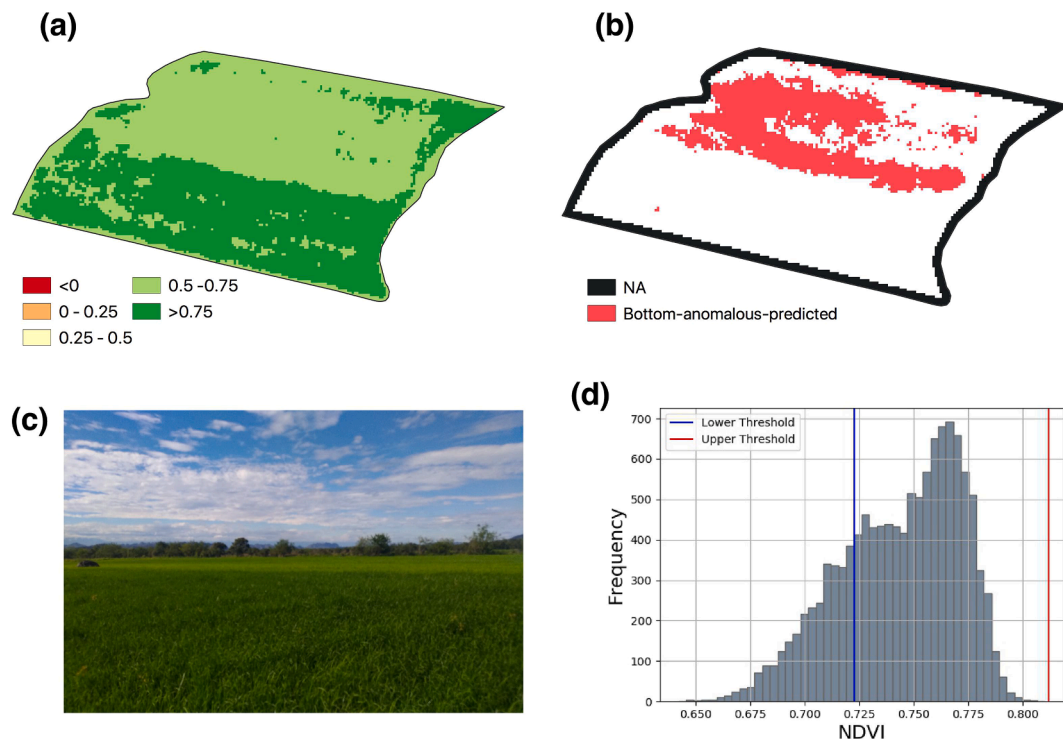
Fig. 15. Results obtained for the PlanetScope NDVI values of a plot with a left-tailed histogram due to the presence of a large anomalous area, consequence of uneven Nitrogen application (a) NDVI values, (b) Anomaly-prediction product, (c) Photography of the plot, (d) Histogram of NDVI pixels.

data were exclusively low-anomalous areas associated with lower canopy density and lower vegetation coverage. Specifically, the success of GNDVI aligns with other studies that identified the GNDVI as better to predict LAI in rice than the conventional NDVI (Wang et al., 2007). As most of the field validation points were registered during the tillering phase, the higher accuracy of SAVI reflects its ability to minimise soil brightness that characterises canopies with intermediate levels of vegetation cover (Huete, 1988), such as rice during the tillering stage.

Most of the Sentinel-2 VIs that produced the highest accuracies are transferable to other systems such as Landsat and PlanetScope, except the reNDVI. However, the results of this study showed that slightly different accuracy scores were achieved when comparing Sentinel-2 and PlanetScope EOAD results applied over the same VIs. Specifically, the

PlanetScope GNDVI did not perform as well as the equivalent for Sentinel-2. This is likely due to the difference in spectral response curve for the green channel, with the PlanetScope channel being much broader (500–590 nm) compared to Sentinel-2 (542–578 nm) (Fig. 16).

A number of the poorer performing VIs are designed to be sensitive to specific absorption features that may be indicative of leaf chemistry or pigments. It is important to note that the ground truth data used in this study related mainly to observations of canopy coverage. Further research should draw comparisons with variables such as Chlorophyll content to assess the capability of the EOAD to indicate, for instance, Nitrogen deficiency, which is known to affect crop productivity as it enhances and stabilises crop growth and yield production (Kuenzer and Knauer, 2013; Wang et al., 2012). In addition, field observations were
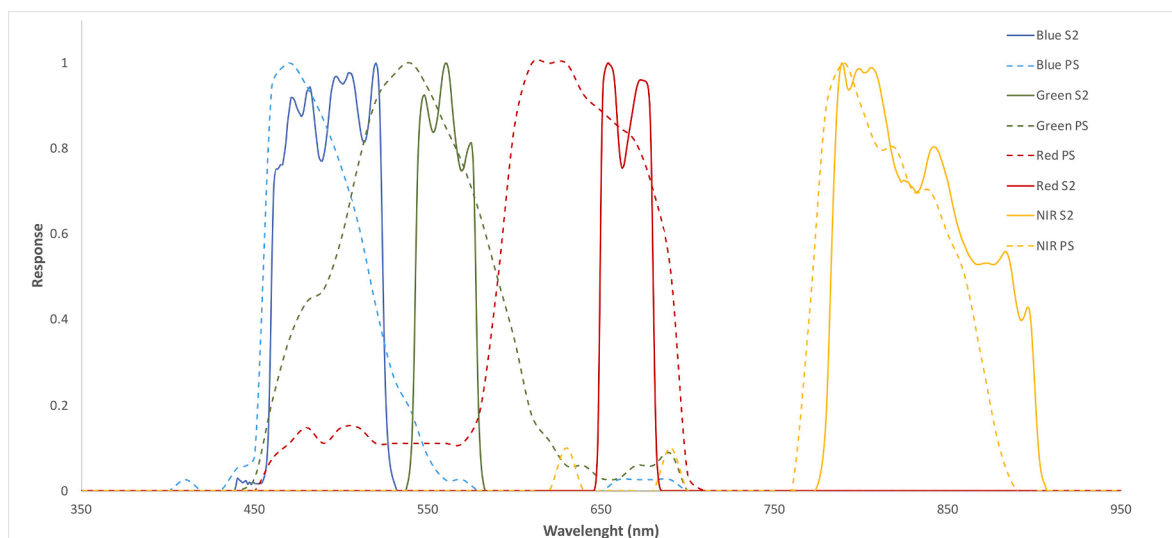

Fig. 16. Sentinel-2 and Planet Scope spectral response functions.

only available for the tillering and booting stage. Future work should consider sampling at different phenological stages to identify the performance of different VI to detect anomalies at each growth stage.

Although the detection of anomalies can provide crucial information for plot-level management decisions, often, PA is focused on the ability of data to indicate or even predict yield. For optical VIs, the occurrence of crop anomalies at different stages impacted the final yield differently. In general, the anomalies identified with the EOAD during later growth stages, using normalised difference indices that included the NIR bands, tended to have a larger impact on the yield for most optical VIs. Particularly, the anomalies that occurred at the booting stage tended to produce significant yield differences between anomalous and non-anomalous pixels in those indices sensitive to chlorophyll. The significant effect of crop condition during the booting stage over yield was also evidenced with the use of average plot VI metrics to predict high/low yield plots. This coincides with the findings of authors such as Chang et al. (2005, 2019, 2017) that indicated a strong relationship between yield and crop condition at the booting stage. This relationship is a consequence of the high Nitrogen (N) absorption rate occurring during this stage (Liu et al., 2016; Xiang et al., 2013). It is during the booting stage that farmers apply nitrogen fertilisers as rice crops demand adequate N supply to maximise yield. Thus, early detection of anomalies during the booting stage is key to implement localised corrective practices but also to identify those plots that require more immediate attention. This, as the inclusion of the percentage of anomalies found with the EOAD improved the prediction of high/low yield plots using the GB classifier. Additionally, the crop anomalies detected during the ripening stage showed a significant relationship with final yield, though at this stage, the crop is in such an advanced state of development that no correct actions can be implemented to optimise the field productivity.

Yields for anomalous pixels (lower values) during the seedling stage tended to be higher when implementing the EOAD on the NDII_b8. Despite the fact that soil water conditions during the seedling stage affect crop establishment (Takeda et al., 2019), no further evidence was found regarding the relationship between crop reflectance and yield at this particular stage. Interviews with local farm agronomist revealed that this behaviour occurs due to the presence of a deeper water layer that delays the emergence of rice plants. However, once the plants emerge, they remain wetter during the whole crop cycle and produce higher yields. Negative NDII values for areas with low LAI can also be an indicator of dry patches and therefore be equally presented as anomalies. Thus, it is required to contrast the NDII_b8_12 surfaces and the anomalous-predicted pixels during the seedling stage to see if the values are positive or negative, the latter representing dry areas that require immediate irrigation.

In terms of the best indices to monitor anomalies in rice plots, SAVI_b8 and GNDVI_b8 showed to be the most accurate at detecting anomalies in the field. The anomalies detected with the GNDVI_b8 also showed a significant negative impact on the yield when detected at the booting stage in comparison to the use of SAVI_b8. Earlier identification of potential underperforming areas can be achieved with the application of the EOAD method using the NDII_b8_11 and NDII_b8_12 at the seedling. These indices did not show a high accuracy to detect anomalies, however, it can be a consequence of the lack of sample points during this particular stage.

5. Conclusion

The EOAD method presented in this paper was able to map anomalies at a sub-plot level in rice crops in Colombia. The success of this approach was evidenced through direct comparisons with in situ observations of anomalies. Detected anomalies can be used to direct farmers to areas of fields to determine what strategy needs to be put in place, such as fixing water supply, to correct for these anomalies bringing about and ultimately an overall improvement to crop yields. Indeed, our study found that areas where anomalies were detected had

significantly lower final rice yields for specific VIs.

The percentage of anomalies detected within the fields also shows to play an important role as a predictor of high/low yield plots at early stages, including seedling and booting. Thus, the EOAD method also allows identifying plots that require more immediate attention and then assess the more problematic areas within the field.

In this study, EOAD was applied to a number of VIs. For the rice crops studied, the use of GNDVI_b8 products produced the best combination of high accuracy and promising detection of potential underperforming areas when implemented at the booting stage. However, future work should include field data at multiple ages during the crop cycle to identify the performance of different VI to detect anomalies at each growth stage and check their impact on yield.

Although this study tested EOAD using just two EO optical data sources, Sentinel-2 and PlanetScope, VIs like GNDVI employ spectral channels common across many EO systems, meaning the EOAD can potentially be applied to imagery from multiple sources, increasing the frequency of anomaly detection. As such, EOAD's ability to be applied to a number of commonly used EO systems means greater observations, thereby providing greater confidence when informing decision-makers on the ground.

Ultimately, the EOAD is designed to be a simple technique, without the need for manual calibration, or indeed, prior expertise in spectral analysis of crops. In this respect, EOAD is applied to histogram data for individual crop plots, in this instance, with data from commonly used VIs (e.g. NDVI, SAVI, GNDVI etc.), derived from freely available EO data. As such, the EOAD approach represents an efficient and low-cost means of collecting PA information almost anywhere in the world. If coupled with automatic approaches for field delineation, this represents an exciting and tractable tool for informing agricultural practices, especially in relatively resource-poor regions of the world where food security is paramount. Although the detection of anomalies can provide crucial information for plot-level management decisions, often, PA is focused on the ability of data to indicate or even predict yield. In general, the EOAD, when applied to high performing VIs (GNDVI_b8, reNDVI_b8_5 and NDVI_b8), demonstrated significant differences in yield between areas that were detected as anomalous and non-anomalous, giving further confidence that the developed method can add value to farming operations using freely available EO data.

CRediT authorship contribution statement

Liliana Castillo-Villamor: Writing - original draft preparation, Conceptualization, Methodology, Formal analysis. **Andy Hardy:** Conceptualization, Methodology, Supervision. **Pete Bunting:** Conceptualization, Methodology, Software, Supervision. **Willian Llanos-Peralta:** Formal analysis. **Miguel Zamora:** Validation. **Yeison Rodriguez:** Validation. **Douglas A. Gomez-Latorre:** Formal analysis.

Declaration of Competing Interest

The authors declare that they have no known competing financial interests or personal relationships that could have appeared to influence the work reported in this paper.

References

Alexandratos, N., Bruinsma, J., 2012. World Agriculture Towards 2030/2015: The 2012 Revision. https://doi.org/10.1016/S0264-8377(03)00047-4.

Allouche, O., Tsoar, A., Kadmon, R., 2006. Assessing the accuracy of species distribution models: prevalence, kappa and the true skill statistic (TSS). J. Appl. Ecol. 43, 1223–1232. https://doi.org/10.1111/j.1365-2664.2006.01214.x http://doi.wiley.com/10.1111/j.1365-2664.2006.01214.x.

Belgiu, M., Csillik, O., 2018. Sentinel-2 cropland mapping using pixel-based and object-based time-weighted dynamic time warping analysis. Remote Sens. Environ. 204, 509–523. https://doi.org/10.1016/j.rse.2017.10.005.

Blaschke, T., 2010. Object based image analysis for remote sensing. ISPRS Journal of Photogrammetry and Remote Sensing 65, 2–16. https://doi.org/10.1016/J.ISPRSJPRS.2009.06.004 https://www.sciencedirect.com/science/article/pii/S0924271609000884.

Bolton, D.K., Friedl, M.A., 2013. Forecasting crop yield using remotely sensed vegetation indices and crop phenology metrics. Agric. For. Meteorol. 173, 74–84. https://doi.org/10.1016/j.agrformet.2013.01.007 https://www.sciencedirect.com/science/article/pii/S0168192313000129.

Bradley, A.P., 1997. The use of the area under the ROC curve in the evaluation of machine learning algorithms. Pattern Recogn. 30, 1145–1159. https://doi.org/10.1016/S0031-3203(96)00142-2.

Bunting, P., Rosenqvist, A., Lucas, R.M., Rebelo, L.M., Hilarides, L., Thomas, N., Hardy, A., Itoh, T., Shimada, M., Finlayson, C.M., 2018. The global mangrove watch - A new 2010 global baseline of mangrove extent. Remote Sensing 10. https://doi.org/10.3390/rs10101669.

Castillo-Villamor, L., Bunting, P., & Hardy, A. (2021). Earth Observation-based Anomaly Detection (EOAD) system. https://github.com/lccastillov/Field_anomaly_detection/tree/v1.0.0. doi:10.5281/zenodo.4753348.

Chang, K.W., Shen, Y., Lo, J.C., 2005. Predicting rice yield using canopy reflectance measured at booting stage. Agronomy Journal 97, 872–878. https://doi.org/10.2134/agronj2004.0162.

Chen, G., Hay, G.J., Carvalho, L.M.T., Wulder, M.A., 2012. Object-based change detection. Int. J. Remote Sens. 33, 4434–4457. https://doi.org/10.1080/01431161.2011.648285.

Delgado, J.A., Short, N.M., Roberts, D.P., Vandenberg, B., 2019. Big Data Analysis for Sustainable Agriculture on a Geospatial Cloud Framework. Frontiers in Sustainable Food Systems 3, 54. https://doi.org/10.3389/fsufs.2019.00054 https://www.frontiersin.org/article/10.3389/fsufs.2019.00054.

Dutrieux, L.P., Jakovac, C.C., Latifah, S.H., Kooistra, L., 2016. Reconstructing land use history from Landsat time-series: Case study of a swidden agriculture system in Brazil. Int. J. Appl. Earth Obs. Geoinf. 47, 112–124. https://doi.org/10.1016/J.JAG.2015.11.018 https://www.sciencedirect.com/science/article/pii/S0303243415300647.

Eerens, H., Haesen, D., Rembold, F., Urbano, F., Tote, C., Bydekerke, L., 2014. Image time series processing for agriculture monitoring. Environmental Modelling and Software 53, 154–162. https://doi.org/10.1016/j.envsoft.2013.10.021.

ESA (2013). User Guides - Sentinel-2 MSI - Processing Levels - Sentinel Online. https://earth.esa.int/web/sentinel/user-guides/sentinel-2-msi/processing-levels.

Freedman, D., Diaconis, P., 1981. On the maximum deviation between the histogram and the underlying density. Zeitschrift für Wahrscheinlichkeitstheorie und Verwandte Gebiete 58, 139–167. https://doi.org/10.1007/BF00531558.

Funk, C., Budde, M.E., 2009. Phenologically-tuned MODIS NDVI-based production anomaly estimates for Zimbabwe. Remote Sens. Environ. 113, 115–125. https://doi.org/10.1016/j.rse.2008.08.015.

Gavioli, A., de Souza, E.G., Bazzi, C.L., Schenatto, K., Betzek, N.M., 2019. Identification of management zones in precision agriculture: An evaluation of alternative cluster analysis methods. Biosyst. Eng. 181, 86–102. https://doi.org/10.1016/j.biosystemseng.2019.02.019.

Gilbertson, J.K., van Niekerk, A., 2017. Value of dimensionality reduction for crop differentiation with multi-temporal imagery and machine learning. Computers and Electronics in Agriculture 142, 50–58. https://doi.org/10.1016/j.compag.2017.08.024.

Hanley, J.A., McNeil, B.J., 1982. The meaning and use of the area under a receiver operating characteristic (ROC) curve. Radiology 143, 29–36. https://doi.org/10.1148/radiology.143.1.7063747.

Henry, C., Daniels, M., Hamilton, M., Hardke, J., 2018. Water Management. In: Hardke, J.T. (Ed.), Rice production handbook chapter 10. University of Arkansas-Division of Agriculture, Little Rock, Arkansas.

Huete, A., 1988. A soil-adjusted vegetation index (SAVI). Remote Sens. Environ. 25, 295–309. https://doi.org/10.1016/0034-4257(88)90106-X https://www.sciencedirect.com/science/article/pii/003442578890106X.

Instituto de Hidrología Meteorología y Estudios Ambientales de Colombia (2020). Sistema de Información para la Gestión de Datos de Hidrología y Meteorología. http://www.dhime.ideam.gov.co/.

Japkowicz, N., & Stephen, S. (2002). The class imbalance problem: A systematic study. Intelligent Data analysis, (pp. 429–449). URL http://citeseerx.ist.psu.edu/viewdoc/summary?doi=10.1.1.711.8214.

Jarrod Hardke, Wamishe, Y., Lorenz, G., & Bateman, N. (2018). Rice Stand Establishment. In Rice production handbook chapter 4. Little Rock, Arkansas: University of Arkansas- Division of Agriculture. https://www.uaex.edu/publications/pdf/MP192/MP192.pdf.

Joint Research Centre of the European Commission (2014). Precision Agriculture: An opportunity for EU farmers - Potential support with the CAP 2014–2020. Technical Report European Parliament.

Kanjir, U.U., urić, N., Veljanovski, T., Duric, N., & Veljanovski, T. (2018). Sentinel-2 based temporal detection of agricultural land use anomalies in support of common agricultural policy monitoring. ISPRS International Journal of Geo-Information, 7. doi:10.3390/ijgi7100405.

Kirova, M., Montanari, F., Ferreira, I., Pesce, M., Albuquerque, J.D., Montfort, C., Neirynck, K., & Moroni, J. (2019). Megatrends in the agri-food sector: global overview and possible policy response from an EU perspective. Technical Report European Parliament, Policy Department for Structural and Cohesion Policies Brussels. URL https://www.europarl.europa.eu/RegData/etudes/STUD/2019/629205/IPOL_STU(2019)629205_EN.pdf.

Koch, B., Khosla, R., Frasier, W.M., Westfall, D.G., Inman, D., 2004. Economic feasibility of variable-rate nitrogen application utilizing site-specific management zones. Agronomy Journal 96, 1572–1580. https://doi.org/10.2134/agronj2004.1572 http://doi.wiley.com/10.2134/agronj2004.1572.

Kuenzer, C., Knauer, K., 2013. Remote sensing of rice crop areas. Int. J. Remote Sens. 34, 2101–2139. https://doi.org/10.1080/01431161.2012.738946.

Lasaponara, R., 2006. On the use of principal component analysis (PCA) for evaluating interannual vegetation anomalies from Spot/Vegetation NDVI temporal series. Ecol. Model. 194, 429–434. https://doi.org/10.1016/j.ecolmodel.2005.10.035.

Le, T.T., Fu, W., Moore, J.H., 2020. Scaling tree-based automated machine learning to biomedical big data with a feature set selector. Bioinformatics 36, 250–256. https://doi.org/10.1093/bioinformatics/btz470 https://github.com/lelaboratoire/tpot-fss.

Lemajic Blanka, S., Pär, V., & Åstrand, J. (2018). New sensors benchmark report on PlanetScope Geometric benchmarking test for Common Agricultural Policy (CAP) purposes. doi:10.2760/178918.

Liang, H., Song, L., Wang, J., Guo, L., Li, X., Liang, J., 2021. Robust unsupervised anomaly detection via multi-time scale DCGANs with forgetting mechanism for industrial multivariate time series. Neurocomputing 423, 444–462. https://doi.org/10.1016/J.NEUCOM.2020.10.084.

Liu, X., Wang, H., Zhou, J., Hu, F., Zhu, D., Chen, Z., Liu, Y., 2016. Effect of N Fertilization Pattern on Rice Yield. N Use Efficiency and Fertilizer-N Fate in the Yangtze River Basin, China. https://doi.org/10.1371/journal.pone.0166002.

Long, J.A., Lawrence, R.L., Greenwood, M.C., Marshall, L., Miller, P.R., 2013. Object-oriented crop classification using multitemporal ETM+ SLC-off imagery and random forest. GIScience and Remote Sensing 50, 418–436. https://doi.org/10.1080/15481603.2013.817150 http://www.tandfonline.com/doi/abs/10.1080/15481603.2013.817150.

Marchesi, C., Thompson, J.F., Plant, R.E., 2010. Factors Underlying Spatial Variability in Rice (Oryza sativa L.) Grain Quality at Field and Regional Level. Agrociencia Uruguay 17, 55–64 http://www.scielo.edu.uy/scielo.php?script=sci_arttext&pid=S2301-15482013000100006&lng=es&nrm=iso&tlng=en.

McCann, C., Repasky, K.S., Lawrence, R., Powell, S., 2017. Multi-temporal mesoscale hyperspectral data of mixed agricultural and grassland regions for anomaly detection. ISPRS Journal of Photogrammetry and Remote Sensing 131, 121–133. https://doi.org/10.1016/j.isprsjprs.2017.07.015.

McKee, T.B., Doesken, N.J., & Kleist, J. (1993). The relationship of drought frequency and duration to time scales. In Proceedings of the Eighth Conference on Applied Climatology. Anaheim, USA,.

Méndez-Vázquez, L.J., Lira-Noriega, A., Lasa-Covarrubias, R., Cerdeira-Estrada, S., 2019. Delineation of site-specific management zones for pest control purposes: Exploring precision agriculture and species distribution modeling approaches. Computers and Electronics in Agriculture 167, 105101. https://doi.org/10.1016/j.compag.2019.105101.

Moldenhauer, K., Counce, P., Hardke, J., 2013. Rice growth and development. In: Hardke, J.T. (Ed.), Arkansas Rice Production Handbook - MP192 chapter 2. University of Arkansas Division of Agriculture, Little Rock, United States of America.

Mondal, P., & Basu, M. (2009). Adoption of precision agriculture technologies in India and in some developing countries: Scope, present status and strategies. doi:10.1016/j.pnsc.2008.07.020.

Mouret, F., Albughdadi, M., Duthoit, S., Kouamé, D., Rieu, G., Tourneret, J.-Y., 2021. Outlier Detection at the Parcel-Level in Wheat and Rapeseed Crops Using Multispectral and SAR Time Series. Remote Sensing 13, 956. https://doi.org/10.3390/rs13050956 https://www.mdpi.com/2072-4292/13/5/956.

Okada, K., & Lopez-Galvis, L. (2018). Improving Resource Utilization Efficiency in Rice Production Systems with Contour-Levee Irrigation in Colombia: Application of Cutting-edge Science and Technology in Developing Countries. In Crop Production under Stressful Conditions: Application of Cutting-edge Science and Technology in Developing Countries chapter 5. (pp. 71–86). doi:10.1007/978-981-10-7308-3_5.

Pérez, A.J., López, F., Benlloch, J.V., Christensen, S., 2000. Colour and shape analysis techniques for weed detection in cereal fields. Computers and Electronics in Agriculture 25, 197–212. https://doi.org/10.1016/S0168-1699(99)00068-X.

Planet Labs (2019). Planet Imagery Product Specifications. URL https://assets.planet.com/docs/combined-imagery-product-spec-final-august-2019.pdf.

Rembold, F., Meroni, M., Urbano, F., Csak, G., Kerdiles, H., Perez-Hoyos, A., Lemoine, G., Leo, O., Negre, T., 2019. ASAP: A new global early warning system to detect anomaly hot spots of agricultural production for food security analysis. Agric. Syst. 168, 247–257. https://doi.org/10.1016/J.AGSY.2018.07.002 https://www.sciencedirect.com/science/article/pii/S0308521X17309095.

Robb, C., Hardy, A., Doonan, J.H., Brook, J., 2020. Semi-automated field plot segmentation from UAS imagery for experimental agriculture. Frontiers. Plant Sci. 11, 1860. https://doi.org/10.3389/fpls.2020.591886 https://www.frontiersin.org/articles/10.3389/fpls.2020.591886/full.

Shaw, D.R., Kelley, F.S., 2005. Evaluating Remote Sensing for Determining and Classifying Soybean Anomalies. Precision Agric. 6, 421–429. https://doi.org/10.1007/s11119-005-3681-9 http://link.springer.com/10.1007/s11119-005-3681-9.

Sokolova, M., Japkowicz, N., Szpakowicz, S., 2006. Beyond Accuracy, F-Score and ROC: A Family of Discriminant Measures for Performance Evaluation. In: Sattar, A., Kang, B.-H. (Eds.), AI 2006: Advances in Artificial Intelligence. Springer, Berlin Heidelberg, Berlin, Heidelberg, pp. 1015–1021.

Takeda, N., López-Galvis, L., Pineda, D., Castilla, A., Takahashi, T., Fukuda, S., Okada, K., 2019. Evaluation of water dynamics of contour-levee irrigation system in sloped rice fields in Colombia. Agric. Water Manag. 217, 107–118. https://doi.org/10.1016/j.agwat.2019.02.032.

Tewkesbury, A.P., Comber, A.J., Tate, N.J., Lamb, A., Fisher, P.F., 2015. A critical synthesis of remotely sensed optical image change detection techniques. Remote Sens. Environ. 160, 1–14. https://doi.org/10.1016/j.rse.2015.01.006.

Tharwat, A., 2021. Classification assessment methods. Applied Computing and Informatics 17, 168–192. https://doi.org/10.1016/j.aci.2018.08.003.

Thomas, N., Bunting, P., Lucas, R., Hardy, A., Rosenqvist, A., Fatoyinbo, T., 2018. Mapping Mangrove Extent and Change: A Globally Applicable Approach. Remote Sensing 10, 1466. https://doi.org/10.3390/rs10091466 http://www.mdpi.com/2072-4292/10/9/1466.

Vories, E., Stevens, W.G., Rhine, M., Straatmann, Z., 2017. Investigating irrigation scheduling for rice using variable rate irrigation. Agric. Water Manag. 179, 314–323. https://doi.org/10.1016/j.agwat.2016.05.032.

Wang, F.-M., Huang, J.-F., Tang, Y.-L., Wang, X.-Z., 2007. New Vegetation Index and Its Application in Estimating Leaf Area Index of Rice. Rice Sci. 14, 195–203. https://doi.org/10.1016/s1672-6308(07)60027-4.

Wang, L., Qu, J.J., Hao, X., Zhu, Q., 2008. Sensitivity studies of the moisture effects on MODIS SWIR reflectance and vegetation water indices. Int. J. Remote Sens. 29, 7065–7075. https://doi.org/10.1080/01431160802226034.

Wang, W., Yao, X., Tian, Y. c., Liu, X. j., Ni, J., Cao, W. x., & Zhu, Y. (2012). Common Spectral Bands and Optimum Vegetation Indices for Monitoring Leaf Nitrogen Accumulation in Rice and Wheat. Journal of Integrative Agriculture, 11, 2001–2012. URL https://doi.org/10.1016/S2095-3119(12)60457-2. doi:10.1016/S2095-3119(12)60457-2.

Wicaksono, P., Lazuardi, W., 2018. Assessment of PlanetScope images for benthic habitat and seagrass species mapping in a complex optically shallow water environment. Int. J. Remote Sens. 39, 5739–5765. https://doi.org/10.1080/01431161.2018.1506951.

Xiang, J., Haden, V.R., Peng, S., Bouman, B.A., Huang, J., Cui, K., Visperas, R.M., Zhu, D., Zhang, Y., Chen, H., 2013. Australian Journal of Crop Science - Effect of deep placement of nitrogen fertilizer on growth, yield, and nitrogen uptake of aerobic rice. Aust. J. Crop Sci. 7, 870–877 https://search.informit.com.au/documentSummary;dn=365115627819305;res=IELHSS.

Ye, X., Kenshi, A.E., Ae, S., Manago, M., Shin-Ichi, A.E., Ae, A., Sasao, A., Ye, X., Sakai, K., Sasao, A., Manago, M., Asada, S., 2007. Prediction of citrus yield from airborne hyperspectral imagery. Precision Agric. 8, 111–125. https://doi.org/10.1007/s11119-007-9032-2.

Zhang, K., Ge, X., Shen, P., Li, W., Liu, X., Cao, Q., Zhu, Y., Cao, W., Tian, Y., 2019. Predicting rice grain yield based on dynamic changes in vegetation indexes during early to mid-growth stages. Remote Sensing 11. https://doi.org/10.3390/rs11040387.

Zhou, X., Zheng, H.B., Xu, X.Q., He, J.Y., Ge, X.K., Yao, X., Cheng, T., Zhu, Y., Cao, W.X., Tian, Y.C., 2017. Predicting grain yield in rice using multi-temporal vegetation indices from UAV-based multispectral and digital imagery. ISPRS Journal of Photogrammetry and Remote Sensing 130, 246–255. https://doi.org/10.1016/j.isprsjprs.2017.05.003.